Grain size effects in hcp polycrystals: from GNDs to blocky alpha

M. A. Cuddihy[1*], Z. Zheng[2], J. Gong[3], T.B. Britton[2], A. J. Wilkinson[3], F. P. E. Dunne[1,2]

1. Department of Mechanical Engineering, Imperial College London, London SW7 2AZ, United Kingdom
2. Department of Materials, Imperial College London, London SW7 2AZ, United Kingdom
3. Department of Materials, University of Oxford, Oxford, OX1 3PH, United Kingdom

Abstract

Typically a 'smaller is strong' size effect is seen when testing objects at the micro and nanoscales. This has significant consequences when using these tests to replicate and understand component level performance, for instance in materials discovery programmes. In this computational plasticity study, we follow the micro-cantilever experimental approach of Gong et al. for determination of size-dependent hcp crystal slip strengths and replicate size sensitivity using length scale dependent crystal plasticity modelling. A fundamental derivation of the back stress term required to harden slip systems according to the mechanism of dislocation pile up is introduced. Model micro-beam single crystals in Ti-6Al under four-point bending were examined which showed that the size-independent slip strength could be correctly determined but that the size-strengthening effect was under predicted. This was attributed to the averaging of discrete dislocation behaviour in to the continuum slip rule required within the crystal plasticity formulation

A systematic study of grain size effects in polycrystal performance has been performed where the grain size was varied from micron scale to millimetres. At the micron scale, length scale-dependent hardening, from the presence of geometrically necessary dislocations (GNDs), leads to classical length scale effects. At longer length scales, such as when the grain size becomes a significant fraction ($1/20^{th}$ or more) of the ligament width, relative geometry effects become significant leading to marked impact on material properties and behaviour. These two bounds provide important contributions to our understanding of component performance and alloy design, particularly in cold dwell facet fatigue in aero titanium alloys and blocky alpha zirconium alloys for nuclear energy.

* *Corresponding author: m.cuddihy12@imperial.ac.uk*

1. Introduction

Understanding the role of materials at the microstructural length scale is critical to delivering the next generation of alloys needs across a wide range of industries. This can either be in leading edge applications, where extracting peak performance is vital such as jet engines, or in increasing requirements for miniaturisation of technology in computing systems, wearable technology, and biomedical tools and implants. Understanding the mechanics at the microstructural length scale for in-service performance plays a vital role in ensuring that these new technologies are fit for purpose and this can be delivered through the parallel development of improved experimental and computational tools. In this study, we provide a systematic case study of size effects and length scale plasticity that can aid our understanding of state-of-the-art micro-cantilever tests and in tandem extend our knowledge to understand critical microstructural features for real-world component performance and lifetime prediction.

For metallic single crystals, the key length scale is often absolute single crystal or grain size, whereas for polycrystals, it is likely both absolute grain size and grain size relative to load-bearing ligament size. The earliest attempt to develop a theory of length scale was the pioneering work done separately by Hall (1951) [1] and Petch (1953) [2], commonly referred to as the Hall-Petch effect. This work linked a range of experimental observations of strength and grain size in mild steel and fitted an empirical relationship:

$$\sigma_y = \sigma_0 + {}^{k}/_{\sqrt{d}}$$

in which σ_y = yield stress, σ_0 = initial strength, k = Hall-Petch slope, and d = average grain size.

Since this work, much more effort has been undertaken to rationalise this across a wide range of material systems and loading regimes. Recent work by Dunstan et al. [3] provides a systematic review of many existing experiments and points out that there is no conclusive evidence for a general inverse square root-dependence of strength upon grain size; rather there are several possible power law fits for various materials. This indicates that the basic premise that ‘smaller is stronger’ and that microstructure refinement is key, however the precise size dependence may vary from system to system depending on the micromechanical mechanism at play.

This recent work highlights the need for new mechanistic insight from appropriate modelling strategies to ensure that experiments are properly understood and enable physical insight to be extended towards service performance. This paradigm shift will enable extension of this mechanistic understanding to complex loading regimes and enable design and lifing engineers to capture state-of-the-art experimental and modelling results appropriately.

Many component designs start with conventional plasticity laws, which are perfectly valid for many types of engineering problems where the dimensions analysed are of the order of millimetres and metres. However, their constitutive behaviour must be informed with empirical data from many curve fits to expensive experimental testing campaigns. One principal weakness is the lack of length scale effects in the constitutive model. This weakness is exemplified in testing with small samples where length scale effects are clearly observed. For example the observed results of a copper wire torsion test performed by Fleck et al. [4], which demonstrated that as the cross-sectional area of the wire was reduced, a strengthening effect may be seen.

These experiments have highlighted the need for a length scale in modern crystal plasticity, and the most prevalent theory to date is the strain gradient theory of plasticity. In this approach, when the length scale associated with deformation is large, and the plastic strain gradient is small, then size-dependent hardening is negligible. Conversely, where high plastic strain gradients exist, at a length scale not insignificant compared to the sample size, then strong size effects develop. A mechanistic understanding of strain gradients has been established by Nye, Fleck, Ashby and others [5]–[8]. They postulate that it is the storage of dislocations that is responsible for accommodating plastic strain gradients that result from inhomogeneous plastic deformation of a crystal (known as geometrically

necessary dislocations or GNDs). Plastic strain gradients, and as such GNDs, result from the geometry of deformation, and they may be observed in a variety of circumstances such as two-phase alloys due to the compatibility of heterogeneous deformation , in micro-indentation or as will be discussed in this work, micro-beam bending. To capture these effects an intrinsic length scale effect is incorporated naturally into a strain gradient crystal plasticity model and this length scale effect is independent of material properties. Much excellent work has been done recently in the computational strain gradient plasticity field; however in the interests of brevity the authors would like to highlight to some of the most significant pieces: [9]–[17].

Recent experimental work by authors such as Gong et al. and Motz et al., [18]–[21] has been on establishing the critical resolved shear stress (CRSS), the threshold stress required for slip to occur on a specific slip system. The use of focused ion beam (FIB) milling in concert with electron backscatter diffraction (EBSD) analysis has enabled the creation of beam samples orientated for single slip on a predetermined slip system. Systematic studies in which the key dimension, beam cross-section width, is progressively reduced have shown that the size dependent contribution to the flow stress scales approximately inversely with the beam width. The explanation provided by Motz et al. for the origin of these effects is that during plastic deformation in single crystal micro-beams, dislocations develop and tend to pileup at a diffuse barrier, the neutral axis, thus creating a back-stress. This pile-up effect has been observed in a recent 2D discrete dislocation plasticity models and analysis by Tarleton et al. [22] and the TEM observations of the dislocations in deformed micro-cantilevers by Ding et al. [23], [24].

Earlier work on micro-columns compressed by indenters has demonstrated size effects which would appear to exist in the absence of strain gradients [25]–[28]. However, these experiments may not necessarily represent a true demonstration of uniaxial deformation behaviour and more complex mechanisms are taking place, such as the development of highly localised slip which leads to high stresses and strain gradients. A potential explanation posed is the 'dislocation starvation mechanism'. It refers to the high surface-to-volume ratio of small samples which allows the majority of the dislocations to escape through the surfaces (starvation); fewer and fewer dislocations remain inside the crystal, prohibiting further plastic deformation. This mechanism may well apply but it is important to note that the micro-pillars in question represent a more complex system than a simple uniaxial compression test. Indeed, most studies neglect to subtract the influence of the substrate on the pillar and as such overestimate the strain such that the pillar acts effectively like a blunt punch [29]. The results must therefore be interpreted in terms of structural size effects, as opposed to just a direct material behaviour. This is emphasised though relatively simple analysis of the length effect scaling, where a simple power law is used for interpreting size effect and this would naturally leading to vanishingly small strengths at the continuum level which are clearly unphysical [19].

In addition to the well-known observations of small-grain size effects, this study is also concerned with large grain effects or relative geometry effects. Again conventional continuum approaches fail to capture the anisotropic effects of crystalline slips and therefore variable components strengths when grain size approaches the component size. This effect is technologically very important, as highlighted with the following three case. Firstly, an in-service issue in zirconium nuclear fuel cladding is the development of blocky-α [30]**.** Blocky-α is α-phase in hcp alloys that is considerably larger and more polygonal than the primary alpha in the sample, quite similar to the large α grains observed in commercially pure titanium. It is thought to arise from exposure in the α phase field, e.g. heat treatments with insufficient deformation such as welding of components. The second area relates to the issue of cold dwell fatigue of titanium alloys, a well-known problem in the aero-engine industry [31]. This phenomenon refers to a reduction in fatigue life as a result of a stress hold in the regular fatigue cycle at ambient temperatures. Empirical and anecdotal evidence from our industrial collaboration [32] suggests a link between large grain size and failure stress.

Finally, the study of the micromechanical behaviour of cardiovascular stents has yielded some research in size effects as related to component ductility [33], [34]. These studies, however, are concerned with relative grain size with respect to component (stent) size; an effect we herein term 'relative geometry'

(as opposed to classical length scale) effect. Interestingly, classical grain size effects are also important in stent applications (for example, [35], [36]) such that in these technological systems, both classical length scale and relative geometry effects are both evident and must be treated appropriately in design and modelling of component performance. It is noted that these stent materials are commonly face-centred cubic stainless steel or cobalt-chrome alloys.

In this paper, we first investigate if dislocation-based length scale crystal plasticity modelling can successfully reproduce the size effects observed in micro-bending experiments and hence whether size-dependent slip strengths may be predicted. We then carry out a systematic study of polycrystal grain size effects, from microns to millimetres, in order to demarcate and to differentiate the various mechanistic contributions in the broad term of "size effects". The polycrystal models, differentiates between what we term "relative geometry effects", i.e. those effects originating from key microstructural features such as grains, with length scale becoming a significant fraction of over 1/20th of stress-bearing ligament size, and the more familiar "length scale effects" which are those introduced through the development of GNDs. Through the systematic study we differentiate between and demarcate the average grain size ranges pertaining to the relative geometry effect and length scale effects. Finally, some examples are discussed of technological significance for which either or both the size effects addressed are relevant and important.

2 Crystal Plasticity Framework

2.1 Slip rule

The crystal plasticity framework utilised in this study has previously seen use in a range of earlier works, for example: [36]–[42], therefore only a brief description will be presented here.

Dislocation pinning is taken to occur through the presence of lattice obstacles, which may include solute atoms, the sessile statistically stored dislocations (SSDs) and their associated structures, as well as GNDs, incorporated in the slip rule as an overall obstacle density. The resultant slip rule determining the slip rate of a given slip system takes the form

$$\dot{\gamma}^i = \begin{cases} 0, & \left|\tau^i\right| < (x + \tau_0) \\ \rho_s^m b^{i^2} \nu \, exp\left(-\frac{\Delta H}{kT}\right) \sinh\left(\frac{\left(\left|\tau^i\right| - x - \tau_0\right)\Delta V^i}{kT}\right), & \left|\tau^i\right| > (x + \tau_0) \end{cases} \quad (1)$$

with

$$\Delta V^i = \gamma_0 \, l b^{i^2}, \text{where } l = \frac{1}{\sqrt{\rho_0}} \quad (2)$$

in which ρ_s^m is the mobile SSD density, ρ_0 the initial sessile dislocation density, b^i the Burgers vector magnitude for slip system i, ν the frequency of attempts (successful or otherwise) by dislocations to jump the energy barrier, ΔH the Helmholtz free energy or activation energy, k the Boltzmann constant, T the temperature in Kelvin (K), τ^i the resolved shear stress, x^i the back-stress on slip system i, τ_0 the size-independent critical resolved shear stress, γ_0 the shear strain that is work conjugate to the resolved shear stress, ΔV the activation volume (note: $\Delta V \approx 18b^3$, consistent with Conrad's range of values for α-Ti [43]) and l the pinning distance. Each slip system becomes active when the resolved shear stress is equal to or greater than the combined effects of the back stress and the size-independent critical resolved shear stress ($\left|\tau^i\right| \geq x^i + \tau_0$). The crystal model is implemented within an Abaqus user-defined element (UEL), which facilitates strain gradient calculations.

2.2 Strain gradients and GNDs

The standard formulation for GNDs relates the closure failure, as defined by Nye [5] (i.e. the discontinuity due to dislocations in a particular plane per unit area), to the gradient of the plastic deformation tensor. This is written here for multiple slip systems:

$$\sum_{i=1}^{n} \boldsymbol{b}^i \otimes \boldsymbol{\rho}_{GND}^i = curl\,(\boldsymbol{F}^P) \qquad 3$$

Therefore the density of GNDs is determined from knowledge of the spatial gradient of the plastic deformation gradient $\boldsymbol{F}^{\boldsymbol{P}}$.

A convenient solution scheme suggested by Arsenlis and Parks is used [8]. Rewriting equation (3), the dislocation density may be phrased in terms of a linear operator $\boldsymbol{A}$, which is the Burgers vector dislocation dyadic terms ($\boldsymbol{d}_i = \boldsymbol{b}_i \otimes \boldsymbol{t}_i$), reassembled into a single matrix:

$$\boldsymbol{A\rho} = curl(\boldsymbol{F^p}) \qquad 4$$

Solution of this equation requires knowledge of the generalised inverse or pseudo-inverse of the $\boldsymbol{A}$ matrix. This is not necessarily a unique problem, as there are may be fewer gradients than there are active slip systems. We choose to use a singular value decomposition (SVD) based pseudo-inverse of the $\boldsymbol{A}$ matrix, which is a specific case of least-squares minimisation. This is relatively straightforward to calculate as each matrix has a SVD, and the inverse is thus:

$$\boldsymbol{A} = \boldsymbol{U\Sigma V}^T \quad , \quad \boldsymbol{A}^{-1} = \boldsymbol{V\Sigma}^{-1}\boldsymbol{U}^T \qquad 5$$

The Fortran library LAPACK was used to calculate the SVD [44]. It should be noted that the dislocation equation represents a potentially over-determined system, and the possibility of a unique solution is limited by the number of terms in the Nye tensor ($m = 9$). Therefore for cases of n slip systems > m, i.e. multiple active slip systems, the solution may be non-unique but will have the minimum least squares difference, as it is the solution of: $min(\|\boldsymbol{A\rho} - curl(\boldsymbol{F^p})\|_2)$.

2.3 Back stress development

In the discussion on potential hypotheses for the understanding of the hardening process in micro-beams, it was stated that dislocations piling up at the neutral axis are believed to generate a back-stress.

The relationship between back-stress and pile-up length was addressed by Motz et al. [21] in the context of micro-beam bending. By considering a single slip plane active in the bent beam, and the two principal forces that act on dislocations on the active slip plane, Motz et al. showed that the pile-up stress, τ_{pu}, or equivalently, back stress, x^i, is inversely related to the pile-up length, L_{pu}:

$$\tau_{pu} = x^i \cong \beta(N) {L_{pu}}^{-1} \tag{6}$$

where $\beta(N)$ is a function of the number, N, of dislocations

In the formulation developed in this paper, the back stress resulting from the build-up of dislocations along an individual prism slip system is established from the analytical approach of Stroh [45].

The shear stress τ_s developing on a slip plane under remote uniaxial loading may be expressed in terms of the number of dislocations, N, the shear modulus, G, Poisson's ratio ν and Burgers vector b and the length of the dislocation pile-up, L_{pu}, (see Appendix A.1 for detail), and is found to be:

$$\tau_s = \frac{GbN}{\pi(1-\nu)L_{pu}} \tag{7}$$

Appendix A.1 presents a validation of this relationship using an independent discrete dislocation plasticity analysis. We estimate the mean free distance between dislocations to be given by:

$$L_f = \frac{1}{\sqrt{\rho_{total}}} \tag{8}$$

such that the pile-up length may be determined from the product of the number of dislocations in the pile-up and the mean free distance from:

$$L_{pu} = NL_f = \frac{N}{\sqrt{\rho_{total}}} \tag{9}$$

Now, using equation 9, equation 7 is re-arranged to yield an expression for the back stress which leads to:

$$x^i = \alpha Gb\sqrt{\rho_{total}} = \alpha Gb\sqrt{\rho^i_{GND} + \rho_{SSD}} \tag{10}$$

where $\alpha = \frac{1}{\pi(1-\nu)}$, which for this material is approximately 0.5.

Equation 10 has the same form as the classical Taylor hardening model but it should be noted that the physical arguments used to derive it are completely different. For the subsequent studies, a distinction in the hardening relation may be made. For the single crystal study, a self-hardening type relation is observed such that the dislocation accumulation on the specified slip system alone contributes to the hardening. However for the polycrystal study, latent hardening is observed such that hardening on slip system *i* increases the slip strength of all other systems.

The GND density is determined from geometry and plastic strain gradients as presented above in Section 2.2. In our single crystal study, the immobile SSD density evolution is taken to be negligibly small, since the experimental single-crystal data show little hardening (see later). However, in the polycrystal studies, some evolution of hardening is observed in independent experiments, and so the density of sessile statistically stored dislocations is allowed to accumulate in proportion to the accumulated slip, p with hardening factor, γ', representing grain boundary interaction effects such that it is nonzero only in the case of polycrystals. The equation is given below (in rate form):

$$\dot{\rho}_{SSD} = \gamma' \dot{p} \qquad 11$$

The hardening factor is chosen to ensure the experimentally observed hardening is reproduced. It is well understood that SSD evolution is a function of plastic slip, however, the precise nature of this function is less clear (and likely varies with temperature, strain rate, and material system). There are limited quantitative experimental techniques and studies of the SSD evolution with strain, as opposed to GNDs where EBSD based methods have shown excellent results [46], [47]. We argue that incorporation of a more complicated evolution rule with additional fitting factors for dislocation density without further mechanistic understanding does not add much value.

2.4 Materials

This work focuses on the near-alpha titanium alloy Ti-6Al which is hexagonal close packed (hcp), and has 24 slip systems. Due to the level of alpha stabiliser in the alloy it is assumed that there is no twinning [48]. The <*a*> and <*c*+*a*> type systems are differentiated (*c/a* ratio of 1.593 is used), and the slip systems for a single hcp crystal are shown in Fig. 1.

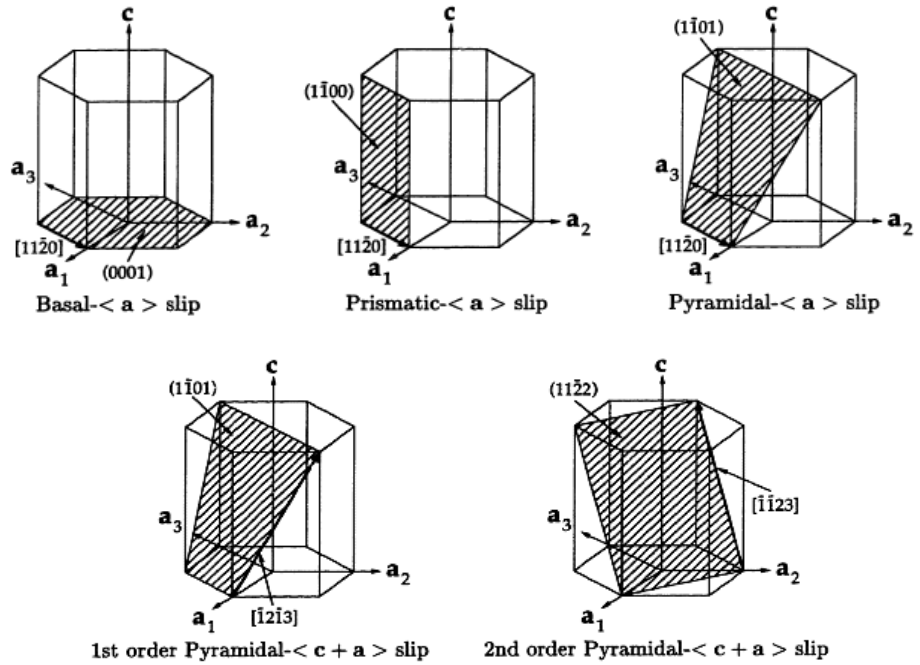

Figure 1 - Hexagonal close packed titanium slip systems [49]

Hasija et al. [50] conducted mechanical tests with samples of single-phase α-Ti–6Al, for both single crystal and polycrystalline samples. The single crystal tests were carried out at constant strain rate, for basal and prismatic slip <a>, and pyramidal slip <c+a>, and the results of these tests established the base critical resolved shear stress; also as hardening is hardly observed in the tests, the hardening coefficient γ' in the SSD hardening rule is set to a small non-zero value of 0.05. The polycrystal tests are compression of samples at three strain rates, 8.4×10^{-4}, 1.5×10^{-4} and 1.68×10^{-5} s^{-1}, and have been used in combination with a representative polycrystal model [51] to determine the activation energy, ΔH, relating to strain rate sensitivity (see Eqn. 1).

Equal strengths are assumed here for basal and prismatic <a> slip systems for simplicity, since the difference between them has been observed to be small in the experiments of Hasija et al. The slip strength of pyramidal <c+a> systems is often observed to be about three times that for basal or prismatic systems, recently demonstrated experimentally by Gong et al [52].

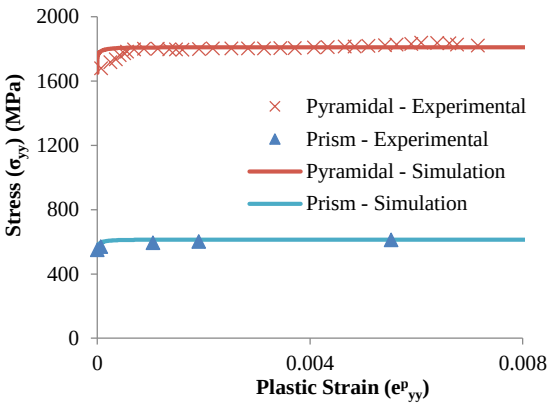

Figure 2 - Experimental and CPFE model curves for prismatic <a> and pyramidal <c+a> slip system response based on single crystal creep experimental data from Hasija et al., [50]

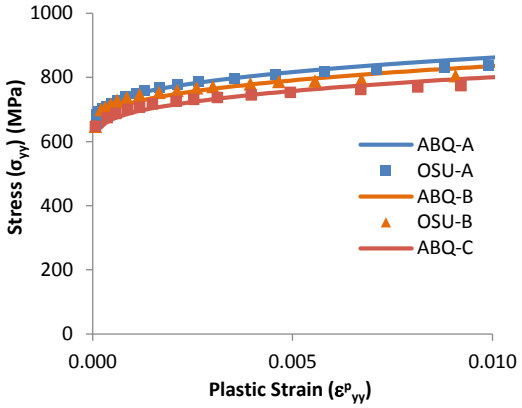

Figure 3 - Strain rate sensitivity calibration results, (ABQ refers to Abaqus simulations [51] and OSU refers to experimental data of Hasija et al., 2003)

The polycrystal model rate sensitivity with an activation energy ΔH = 9.91x10^{-20} J/atom is shown for the three strain rates indicated in Fig. 3, providing a good representation of the polycrystal average stress-strain response. The small amount of strengthening observed is captured simply by means of the contribution from grains badly orientated for slip within the polycrystal, such that the hardening factor, γ' remains as would be expected from the single crystal tests. Latent hardening is considered for the polycrystal models such that hardening on the i^{th} slip system increases the slip strength of all other systems. Elastic moduli and slip rule constants for the representative Ti-6Al are given in Appendices A.2 and A.3 respectively.

3 Micro-beam bending analysis: the classical length scale effect

The micro-cantilever experiments described by Gong et al. [18], [19], [52], [53] serve as the basis for this section of the study.

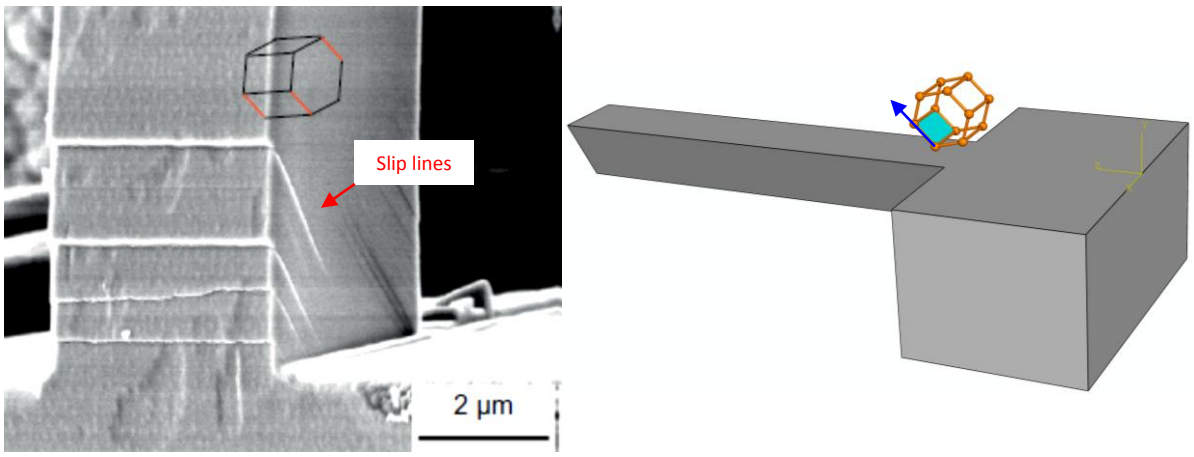

(a) (b)

Figure 4 – (a) In-situ image of development of well-ordered slip on the <a> prismatic system (b) schematic of beam studied [53]

In their work, regions in various single crystal titanium and zirconium alloys were selected by EBSD so that the resulting beams would activate individually specified slip systems. FIB milling techniques were used to machine out triangular cross-section beams, where the depth of the beams range in a

decade of sizes all less than 20μm. The ratio of length to depth is maintained at 6:1 to ensure that manufactured beams are commensurate with Timoshenko classical beam theory and thus reducing contributions of compliance within the 'built-in' end, which is explicitly modelled, and simplify the analysis. The samples are then passed to a nano-indenter that applies a displacement to the free end of the cantilever. Load-displacement data is generated in each case, such that a systematic comparison may be generated for either different cross-section sizes, different representations of alloys [19], chemical effects [54], or perhaps a particular slip system [24]. These observations all include a general trend that 'smaller is strong' due to length scale effects.

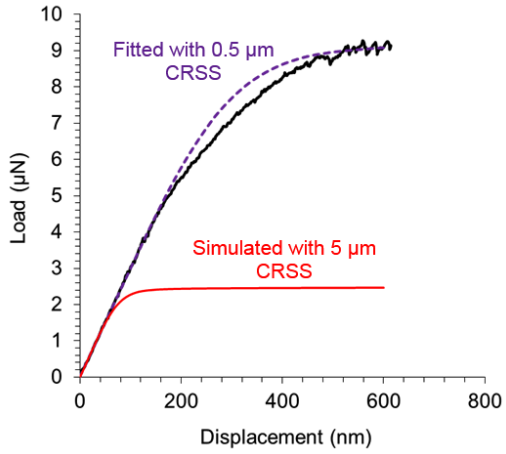

Figure 5 – Load-displacement data from micro-cantilever testing of pure zirconium. Results from 0.5μm cross-section width cantilevers. Black curve is the experimental result, dashed purple line is CPFE fitting and red curve is a comparison using τ_0 from 5 μm <a> prismatic beams [53]

Each cantilever beam is explicitly modelled with a different length scale CPFE simulation to generate force-displacement data which are then matched with the experimental data until a good fit is reached, after varying the threshold resolved shear stress (τ_0) in the CPFE model. Fig. 5 shows an example of this process, in which the purple dashed line represents the best fit to the experimental results, as opposed to the red line, which is the force-displacement data generated from a CPFE model with a very different and inappropriate value of τ_0. As this approach to extract τ_0 uses a length scale independent model, values of τ_0 have been extracted and then a description of the size effect based upon the work of Motz et al. has been used to extract bulk flow stresses and the scaling parameter, according to the equation: $\tau_f = \tau_0 + {}^{A}/_{d}$.

As a complementary contrast, it would be useful to include an explicit length scale dependent crystal plasticity model to simplify fitting and improve our confidence in the underlying model. In this study we start with our proposed length scale dependent (GND-based) model to generate some force-displacement curves for a range of object sizes. We then follow a similar approach to Gong et al. and use a length scale *independent* model to fit force-displacement curves. This second fitting extraction of size-dependent slip strengths and then post-facto comparison to length scale models and thereby provides a thorough test of the length scale dependence of the crystal model in predicting size-dependent slip strengths.

In experiment, cantilevers are used as they are simple to manufacture and test. Choice of a bend geometry in both cases is required to create a soft pile-up and resulting back stress, resulting in the bending size effect. The size of this back stress is amplified when the strain gradients are increased. These effects are also seen in real microstructures, where refinement in grain sizes results in larger strain gradients and therefore, hardening. Here we use four-point bending test specimens in the CPFE model as this provides a simple mechanical test object to analyse and rigorously discuss. The particulars of this choice are discussed below.

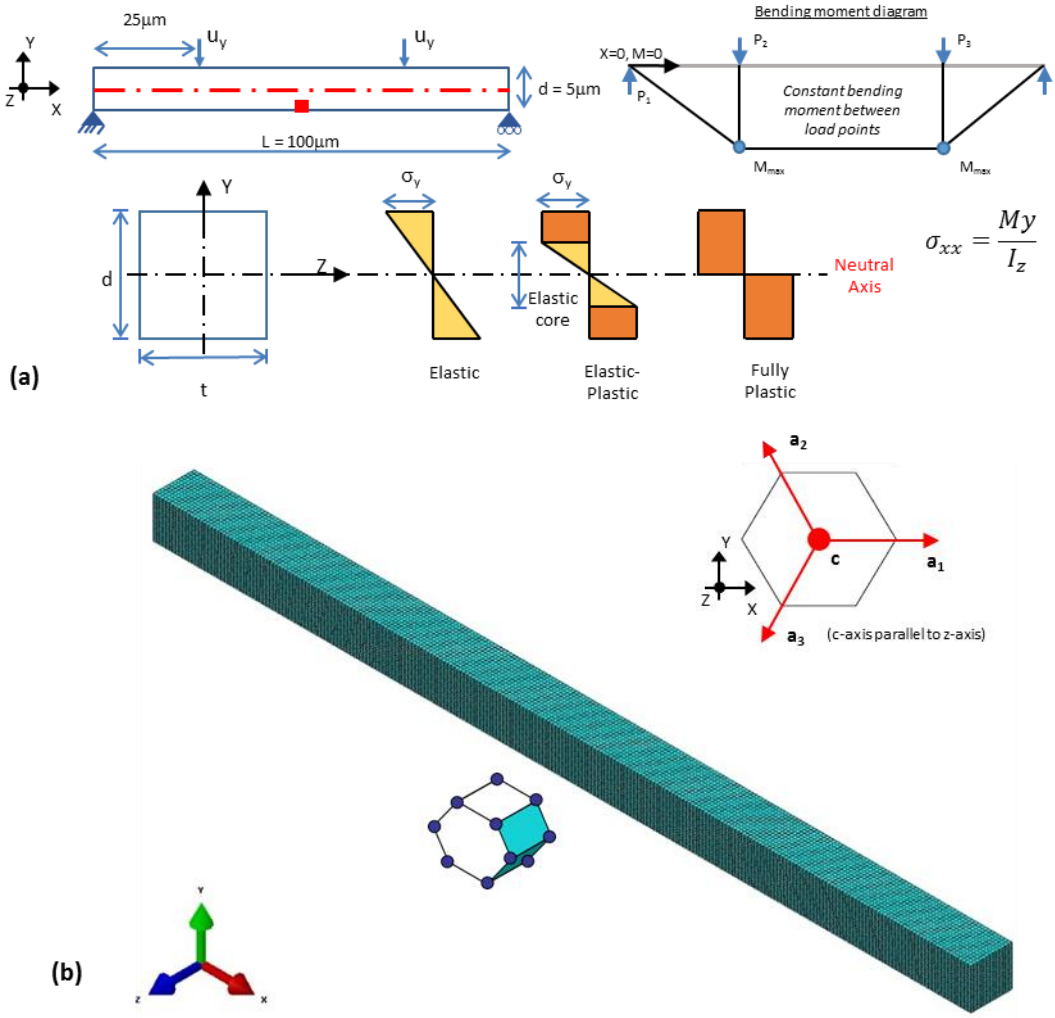

Figure - 6(a) Four point bending beam, square cross-section and schematic representations of the development of plasticity in beams (b) Beam mesh used for CPFE simulations

Under four-point bending, beams undergo constant bending moment between the loading points, as indicated by the diagram above (Fig. 6(a)). Along with constant moment, there is constant bending stress and with an appropriately dimensioned beam (length ~ 20 x height), linear variation of stress through the mid-line, which coincides with the neutral axis. Shear is thus minimised due to the use of sufficiently long beams (as with the cantilever study). Under plasticity (shown as perfect plasticity for simplicity in the schematic) the stress variation through the mid-section is as shown in Fig. 6(a).

A range of single crystal beams sizes are considered: 1, 2.5, 5, 10, 15, 20, 100, and 200µm. In each case mesh element resolution remains the same as the only difference is that nodal coordinates are scaled appropriately to give the required size. Mesh resolution is required to be fine, and in each case over 95,000, 20-node hexahedral elements were used[†], as shown in Fig 6(b). The crystallographic orientation of each beam remains the same and has been chosen to ensure slip on two identical prismatic systems (due to the symmetry of the reference configuration of the hcp crystal). This specified crystallographic orientation is shown schematically in Fig. 6(b).

[†] *Proper execution of the GND calculation requires very fine spatial and temporal resolution, i.e. resolution of the mesh and the time steps in the integration procedure respectively; this relatively large problem was tackled by the parallel direct sparse solver in Abaqus/Standard utilising a HP Z620 workstation with an Intel Xeon E5 3.60GHz multi-core processor and 32.0GB RAM*

Each model is executed with GND evolution and consequent hardening as described previously, and the model parameters are given in the Appendix. The beams are displaced at the points indicated in Fig. 6(a) until a significant amount of plasticity occurs. These models form the 'pseudo-experimental' data set. The purpose of this study is to examine whether similar behaviour may be observed as in the cantilever micro-mechanical experimental tests.

The pseudo-experimental force displacement curve is fitted with a curve generated by size-independent crystal plasticity until good agreement is reached, in the same manner as the cantilever experiments. The results obtained are shown in Fig. 7, and note that they are presented in terms of normalised bending moment and normalised displacement for comparison convenience. Normalised bending moment is given as:

$$M^* = \frac{M}{bt^2}, \text{ where M=(force) x (lever arm)} \qquad 12$$

Normalised displacement is simply the displacement at a point in time divided by the maximum displacement (the displacement applied to each beam varies appropriately with the cross-section size). Fig. 7 (a) – (h) show normalised bending moment versus normalised displacement for a range of beam cross-section size (1μm to 100μm). Solid black lines show the size-independent CP normalised bending moment results for values of τ_0 which form upper and lower and bounds about the pseudo-experimental results, which are shown by the black star symbols. The red square symbols correspond to the best fit size-independent CP model results from which the corresponding size-dependent slip strength is then extracted, and given in the figures.

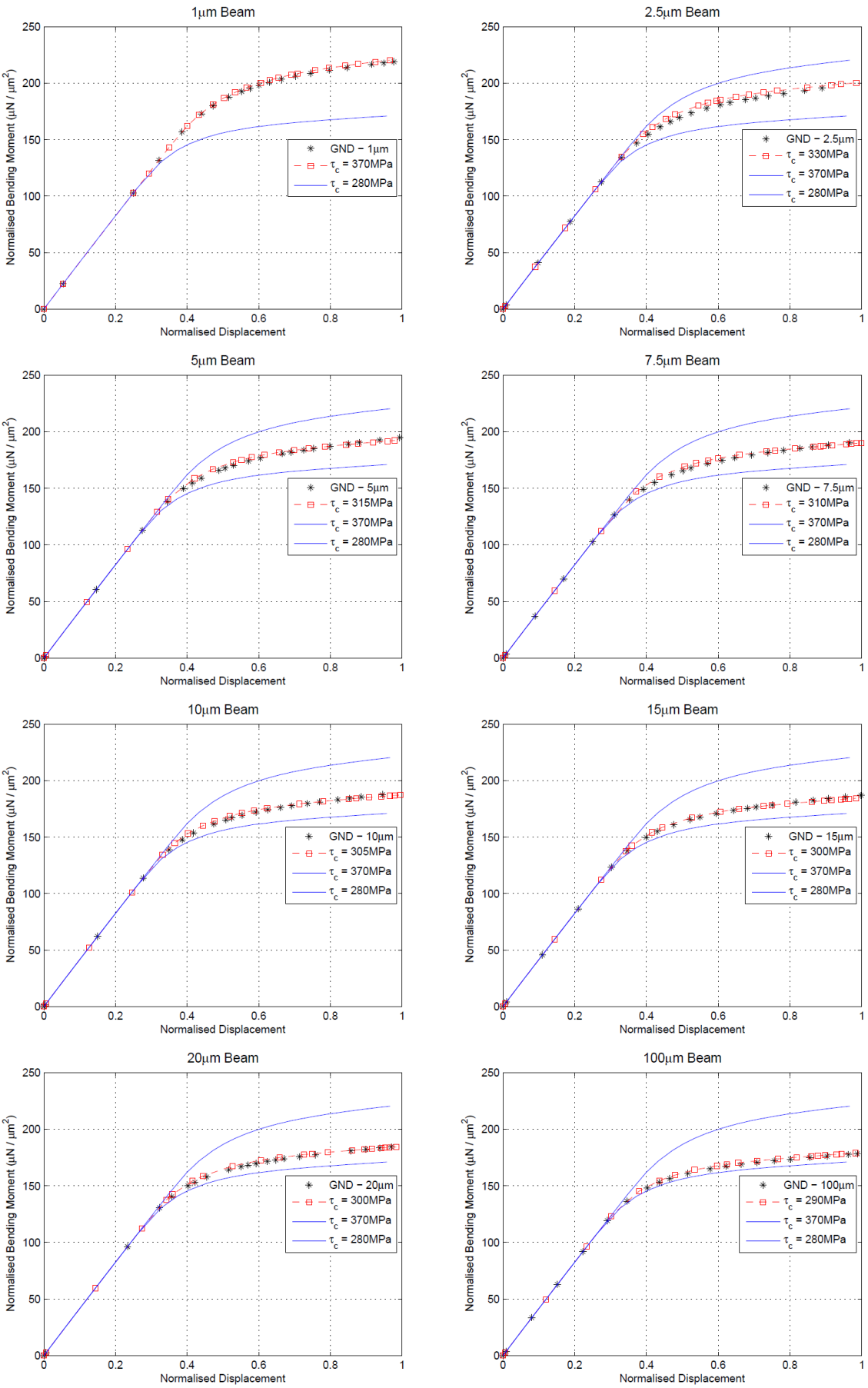

Figure 7 – Size independent CPFE comparisons with the 'pseudo-experimental' GND models

It is argued throughout this paper that the development of GND densities contribute to the hardening observed at small length scales and are thus key to understanding the size effect. Thus it is prudent at this point to examine GND activity in more detail.

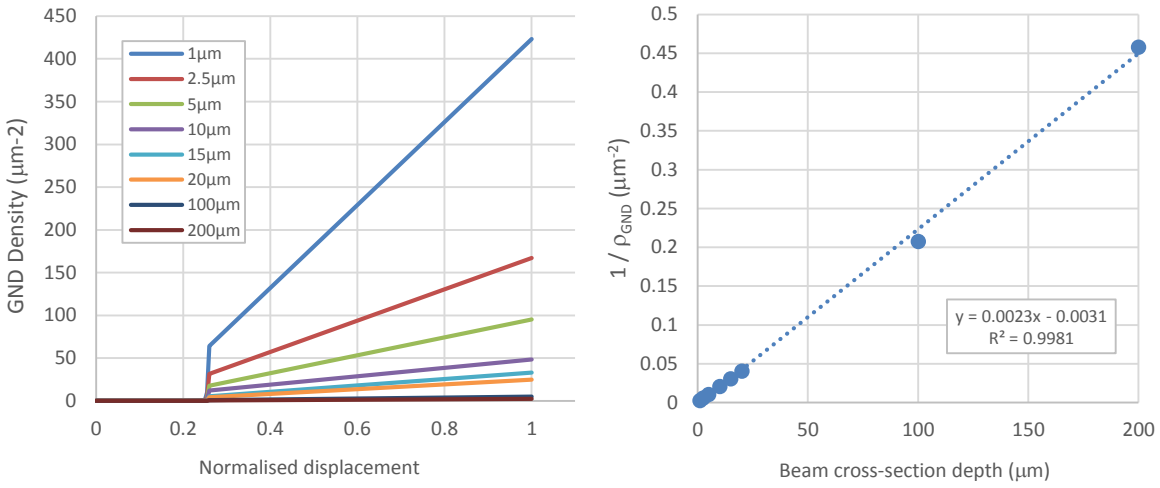

(a) (b)

Figure 8 - (a) GND evolution in beam midpoint over time, refer to Fig. 6(a), which highlights this location with a red square and (b) GND density at end of loading, compared with cross-section depth

Consider the two figures 8(a) and 8(b). Fig. 8(a) shows the development of GND density versus normalised displacement for each beam. Early stages of the analysis remain elastic therefore giving zero GND density, as GNDs are required only to support plastic strain gradients. Once the stress at the extreme fibres is such that plasticity occurs, owing to the nature of beam bending, a plastic strain gradient is induced and GND density develops accordingly. A very strong relationship between cross-section size and plastic strain gradient magnitude results, and this point is very clearly illustrated in Fig. 8(b). This figure shows the GND density at the end of the displacement, and the magnitude of densities is shown to be minimal once a beam width of ~10µm is achieved, i.e. the GND density in the 1µm beam substantially exceeds that of the 100µm beam. The length scale crystal model therefore provides the argument that size effects are really only apparent in sample sizes less than ~20µm. An inverse relationship is observed to hold between the GND density and the cross-section depth.

The size-dependent values of slip strength are then collated, and plotted against beam cross section-depth in Fig 9(a). The data are then fitted with a curve: $\tau_0 + {}^{A}/_{d^n}$, with A=97, n=1, giving a size-independent prism slip strength of τ_0=287MPa. The corresponding results obtained in the experiments of Gong et al [9,10] are shown in Fig 9(b), showing the same size-independent slip strength, but giving a much higher sensitivity to beam size, or strength parameter, A=354. Motz et al [21] also determined a much higher strength parameter but for copper, shown in Fig. 9(c).

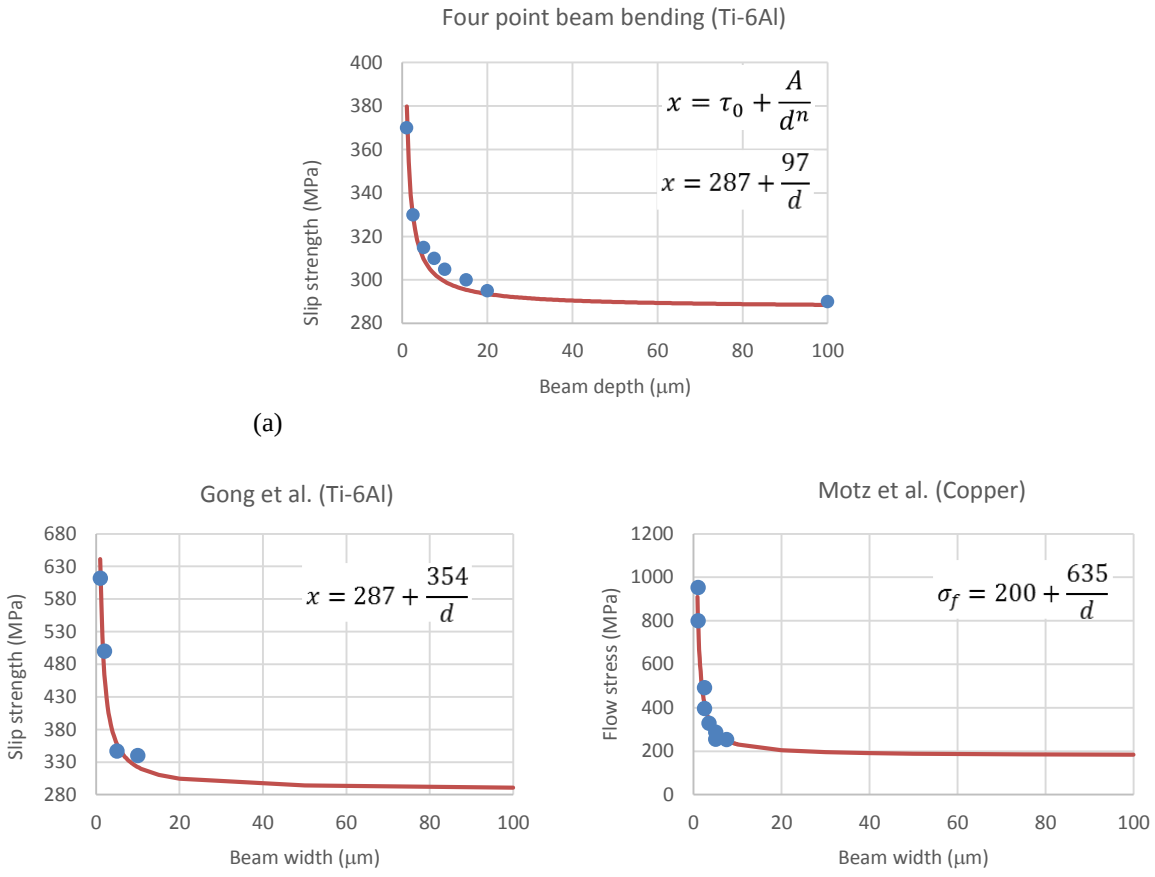

Figure 9 - Scale-dependent slip strengths versus micro-beam depth (a) determined from length scale crystal plasticity for model Ti-6Al, (b) from experiments and CP modelling by Gong et al. [19] and (c) by Motz et al. [21] for pure copper.

The difference between the CPFE determined and measured strength parameters for Ti-6Al likely originates from the hardening model derived in Eqn. (10). The back stress development on an individual prism slip system is mechanistic and has been validated using discrete dislocation plasticity. However, it is implemented within a continuum crystal slip model in which the discrete nature of the dislocations is then lost.

This section addressed classical length scale effects through evolution of GNDs supporting plastic strain gradients. These are predominantly associated with fine grain microstructures, but as grain size increases, so these effects diminish such that polycrystal behaviour tends to become size independent. However, with further increasing grain size with respect to fixed sample geometry, ultimately a further size effect becomes significant, in which behaviour becomes critically dependent on the local microstructure features (e.g. grain orientation, or morphology). In order to differentiate this effect from the classical length scale effect, we label it the relative geometry effect and it is explored further in the next section.

4 Polycrystal studies: classical length scale to relative geometry effects

As mentioned in the introduction, it is now of key industrial interest to examine the behaviour of polycrystals with a range of grain sizes, whether to critically assess the strengthening effects of small grain size or the potential deleterious impact of large coarse grains in a sample or component (for example, occurring in blocky alpha zirconium).

This study seeks to address a broad spectrum of grain sizes, from the micron scale, below 10μm, for which classical length scale effects pertain, through to large grains, of the order of millimetres, with respect to a fixed sample size for which a millimetre-sized grain begins to form a significant fraction (e.g. >10%) of the load-bearing ligament width. The nature of the study is described schematically in the figure below.

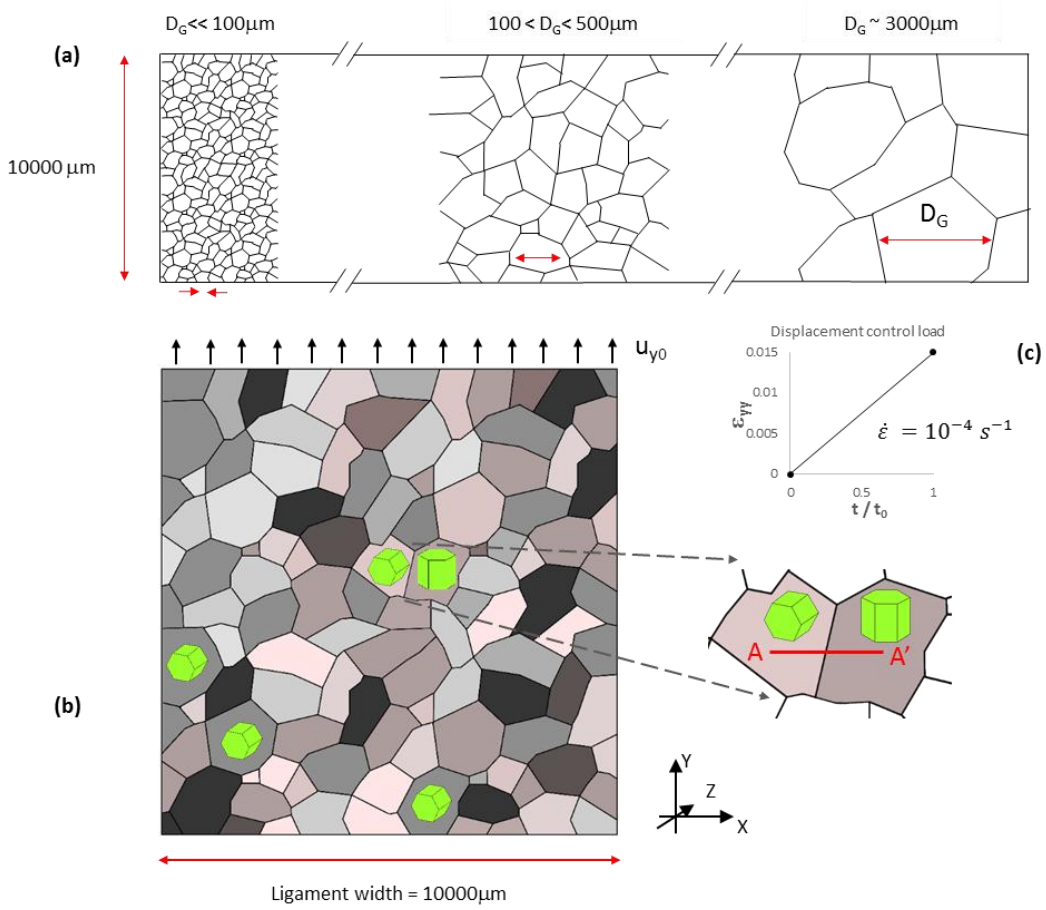

Figure 11 - Polycrystal model schematic outline, (a) illustrating the definitions of fine, medium and coarse grains (b) a typical polycrystal representation and the location of the embedded 'rogue pair', and (c) the displacement-controlled loading, macro strain

We consider a representative HCP polycrystal sample with fixed in-plane ligament width of 10000μm, subject to uniaxial displacement controlled loading up to 1.5% strain, in which the effect of changing average grain size is investigated. Fig. 11 indicates the range of average grain size considered, showing schematically a fine grain size with many thousands of small grains within the ligament width, through to large grain size of order 3000μm. The extreme coarse 'average' grain size is that for which the grain size is equal to the ligament width; i.e. the polycrystal has reduced to a single crystal. We anticipate three distinct regimes: (i) fine grain size leading to length scale effects, but for which a representative volume element (RVE) has been established, (ii) a medium grain size with respect to ligament width for which the length scale effect has become negligible but for which an RVE has still been maintained,

and (iii) large grain size for which no classical length scale effect exists, but an RVE is no longer maintained, such that the response of the sample becomes crucially dependent on local crystallographic orientation and grain morphology. The latter case we refer to as relative geometry effects (to differentiate from size effects) and is representative of blocky alpha zirconium in small ligament widths for which large property variations (yield, strength, fracture) result from small variations in microstructure.

The aim of the study is to establish the demarcations between the three regimes, and to provide guidance on the average grain size (with respect to ligament width) for which length scale or relative geometry effects become important in influencing material response. Naturally, the study is confined to single-phase HCP polycrystals for grain size distributions with small standard deviations, though aspects of extreme in-sample grain size variation are addressed later. This study addresses microstructure quantities thought to be far more sensitive indicators of local behaviour. Particularly, we consider a combination of two grains buried within the polycrystal orientated such that one is favourable for slip and the other is not; this grain couple is indicated in Fig 11(b), and path AA' indicates where key stress magnitudes are extracted for analysis. Fig. 11 shows grains in 2D but the model is fully pseudo-3D, i.e. grains have a directionally solidified structure and rectangular morphology, giving prismatic grains, such that the geometry of the grain morphology varies on the x-y plane and all grains have the same depth in the out of plane direction. The nature of 'realistic' grain morphology has been addressed by Sauzay and co-workers [55] who have found that it contributes little to the overall mechanistic behaviour.

Each polycrystal model developed for the study, typically having a different average grain size, requires a different finite element mesh, and care has to be taken to ensure that the mesh resolution is consistent throughout, but particularly for the grain couple and immediately surrounding grains under analysis. Apart from the grain couple with specific misorientation, all other grains in the model are assigned pseudo-random orientations, but with the imposed constraint of having c-axes inclined to the remote loading direction at an angle > +/-20^{o} in order to favour slip. The material properties and slip rule are identical to those utilised for the single crystal Ti-6Al study earlier.

4.1 Relative geometry effects

Firstly, larger average grain size models are examined. These represent samples of average grain size of between approximately 800 to 3000μm, leading to within 12 to 130 grains in the model with a consequent 3 to 10 grains within the sample ligament width. With these large grain sizes with respect to the sample ligament width, it becomes clear that it is the ratio of grain size to ligament width which is key in determining material behaviour.

Macro stress strain curves for these polycrystals are shown in Fig. 12 for two cases. Firstly, Fig. 12(a) shows the stress strain curves for various differing numbers (from 12 to 132) of grains in the polycrystal.

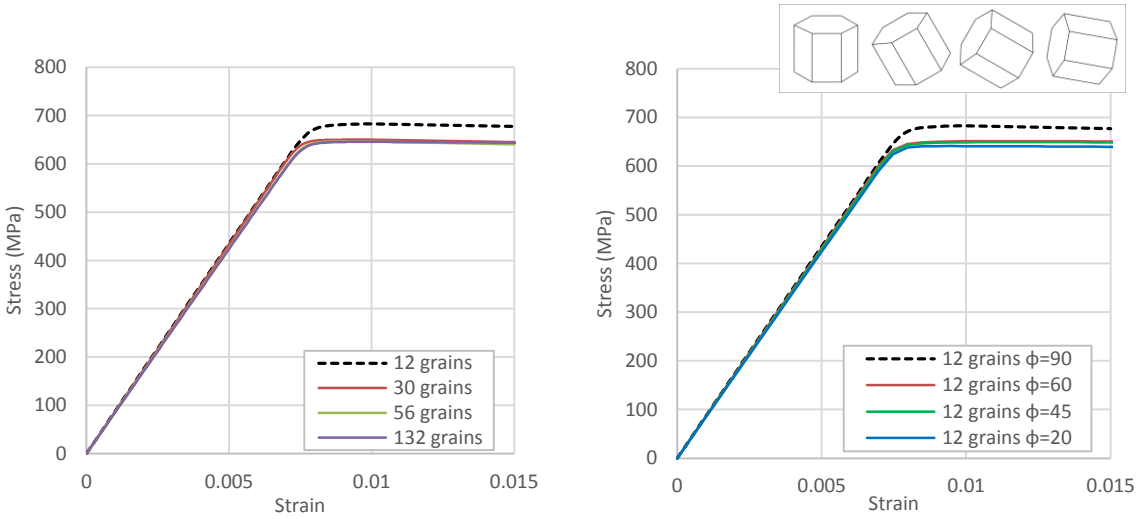

(a) (b)

Figure 12- Macro stress strain responses for: (a) number of grains in polycrystal model (b) rotation of hard unit in 12 grain model

Macro response converges quickly – only 30 grains are required after which the addition of further grains has no significant impact on the macro response, which tends to approximate to that of single crystal behaviour when orientated well for slip (with a tensile strength of ~650MPa). However, one of the centrally-based grains (see Fig 11(b) for schematic) in the twelve-grain model (i.e. very large grain size) is then progressively rotated away from a hard orientation (with all other microstructural features remaining the same) leading to the macro-response shown in Fig 12(b). Modest variation in macro-level stress response is therefore seen, but locally, at the boundary of the rotated grain, very much more significant change occurs, and this is addressed next.

Consider the graphs in Fig. 13, which show distributions of both yy-stress and accumulated plastic strain along the path AA', which passes through the grain couple shown schematically in Fig 11(b), for which one of the grains is orientated badly for slip (c-axis parallel to loading), while the second is well-orientated for slip.

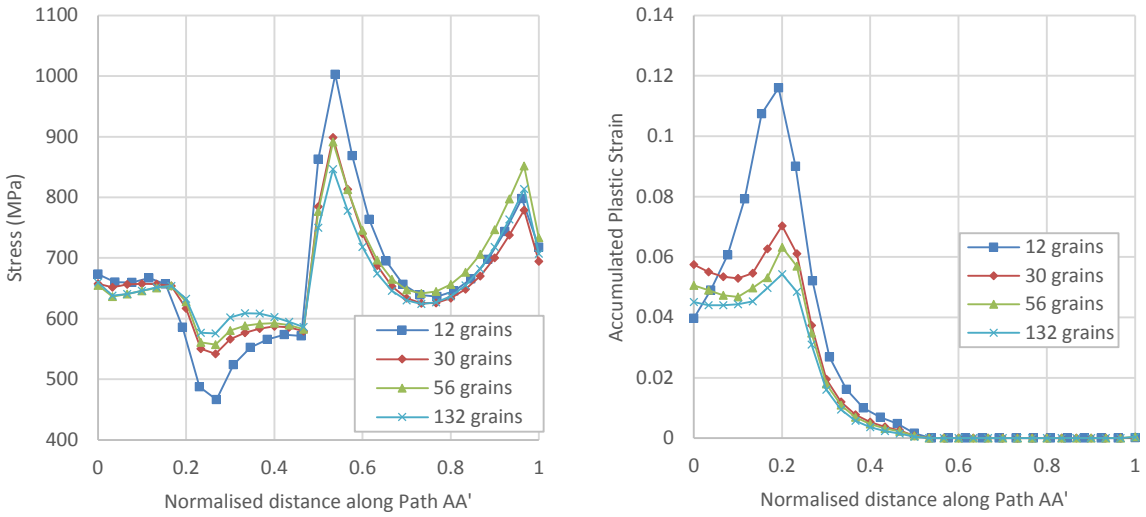

Figure 13 – Effect of relative geometry on (a) Stress (σ_{yy}) and (b) Accumulated plastic strain (p) along Path AA'

The macro stress strain curves (Fig 12(b)) would not seem to indicate much of a grain size effect, however of more significance is the local stress and plastic strain development, at the boundary of the soft-hard grain pair. Considering Fig. 13(a), there is considerable stress redistribution from the soft grain onto the hard grain, and the peak boundary stress difference from the coarsest to a finer grain size is almost 150 MPa. This occurs because of the load sharing between hard and soft grains and, as the grain size increases with respect to fixed sample ligament size, so the balance changes because of the increasing role of free boundary effects. Fig. 13(b) shows the accumulated plastic strain, *p*, distributed along path AA', given by:

$$p \equiv \int_0^t \sqrt{\frac{2}{3}(\dot{\boldsymbol{\varepsilon}}^p : \dot{\boldsymbol{\varepsilon}}^p)}\, \mathrm{d}t \qquad 13$$

The soft grain in the coarse grained sample accumulates a very large amount of plastic strain, locally, compared with the overall macro applied strain of ~1.5%. The increase in local strain with increasing grain size results from the smaller proportion of plastic load-bearing capacity, since the badly orientated grain does not deform plastically. As the number of grains in the polycrystal increases so the local plastic strain in adjacent softer grains decreases. This relative geometry effect occurs only because the grain size forms a significant fraction of the sample ligament width. A useful question, therefore, to address is what is the critical grain size, with respect to ligament width, for which this phenomenon is observed to occur, since it is likely to have significant implication for homogeneity of deformation, strength and fracture properties, and this is addressed shortly. However, next, the classical length scale effect in polycrystals is briefly summarized in order to enable the range of polycrystal deformation from fine to coarse grain size to be unified.

4.2 (Classical) length scale effects

From the previous study, it is seen that as the grain size diminishes with respect to the ligament width, so the relative geometry effect diminishes away such that local, grain-level stresses become independent of grain size. This point is observed when the average grain size (AGS) is approximately 1/20th of the sample ligament width. However, as the average size continues to decrease, size effects resulting from the establishment of plastic strain gradients supported by GND development, begin to influence local stresses through slip system hardening

The earlier single crystal study, beam bending, showed that for beam widths of greater than about 100μm, there was found to be low GND density development. Therefore this polycrystal study pursues grain size down to the micron level in which size effects are known to be of significance, within the 1-50μm ranges. The establishment of the representative polycrystal model shown in Fig. 11 with AGS 1μm would lead to models containing ~4 million grains. This is not realistically achievable with practical computing resource, and as a result, utilising the knowledge of the necessary model size with respect to given AGS to eliminate relative geometry effects, we establish a series of dimensionally scaled sub-models with varying AGS 5, 10, 15, 30, 100, and 200μm respectively. In the same way as for the study in Section 4.1, the local stresses at the boundary of a grain couple badly and well orientated for slip respectively are examined, and shown in Fig 14(a), together with local GND density distributions along the path AA' in Fig 14(b), for the AGS shown.

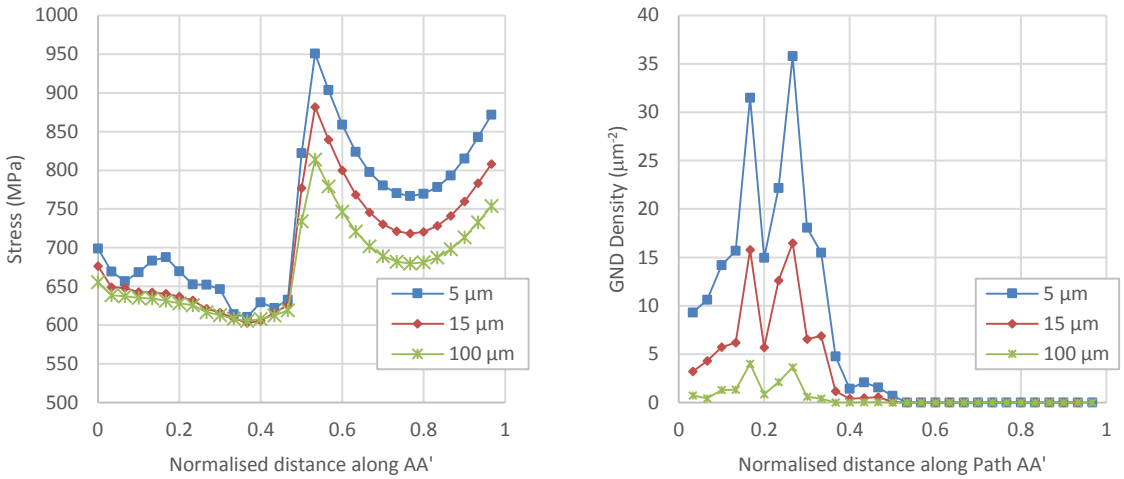

Figure 14– Length scale effects demonstrated for three average grain sizes, 5, 15, and 100μm, with (a) stress (σ_{yy}) and (b) GND accumulation along Path AA'

The GND density is of the anticipated magnitude of ~10μm^{-2} (i.e. 1x10^{13} m^{-2}) as would be expected from micro-beam studies. A consequence is the increase in local grain boundary stress with decreasing grain size, resulting from the classical length scale effect.

Hence, in summary, in the model single-phase polycrystals examined in Sections 4.1 and 4.2 in which AGS is varied from microns to millimetres in a sample of fixed ligament width of 10,000μm, scale effects of differing physical origins play a role particularly at the extremes of AGS. At small absolute grain size, classical length scale effects are important, but for coarse AGS (with respect to the ligament width), relative geometry effects predominate in controlling properties and behaviour. In the next section, we therefore attempt to unify the results from above for the complete range of grain sizes in order to demarcate the key separations and dominances occurring in model polycrystal deformation.

4.3 From length scale to relative geometry effects in polycrystals

A systematic study over the range of grain size is carried out. This focusses particularly on local microstructure-level grain couple boundary stresses as before in order to draw comparisons. This covers a range of grain sizes from 5μm up to coarse grained and includes single crystal behaviour. A length scale dependant crystal plasticity model has been used.

The results obtained for this systematic study are shown in Fig. 15(a), together with a schematic demarcating the key grain size ranges in Fig. 15(b). Starting at the fine-grained region, local grain boundary stress is dependent on grain size from classical length scale effects. As the grain size increases, so the local GND hardening diminishes and the local stress decreases and saturates at the length scale independent level at an effective AGS of about 20μm. No substantial change to local stress emerges

then until the AGS has increased to a level of about 500μm. The magnitude of this critical AGS depends on the sample ligament width (here 10,000μm) so that this demarcation is relative and not absolute in the sense of length scale effects. The key quantity determining the demarcation is the ratio of grain size to ligament width, which is about 1/20th. After this AGS, the local stresses, and indeed material properties such as yield, strength and fracture become highly sensitive to the details of the microstructure.

In order to demonstrate this, for several polycrystal models with large AGS, the badly orientated grain in the grain couple is systematically rotated (as indicated by the symbols and crystal schematics in Fig 15(a)) and the local boundary stresses determined. These are also shown in Fig 15(a) for AGS larger than about 700μm, and the sensitivity to microstructure becomes clear, and of course is seen to increase dramatically as the AGS increases. The local stress results for increasing AGS are bounded by two extreme cases; those of single crystal response with HCP crystal c-axis normal and parallel to the applied loading respectively, and these two points terminate the graph for 'AGS' of 10,000μm. The extremes result from the slip strength anisotropy in Ti in which typically slip strength differences may be expressed τ_0 <c+a> = 3 * τ_0 <a>.

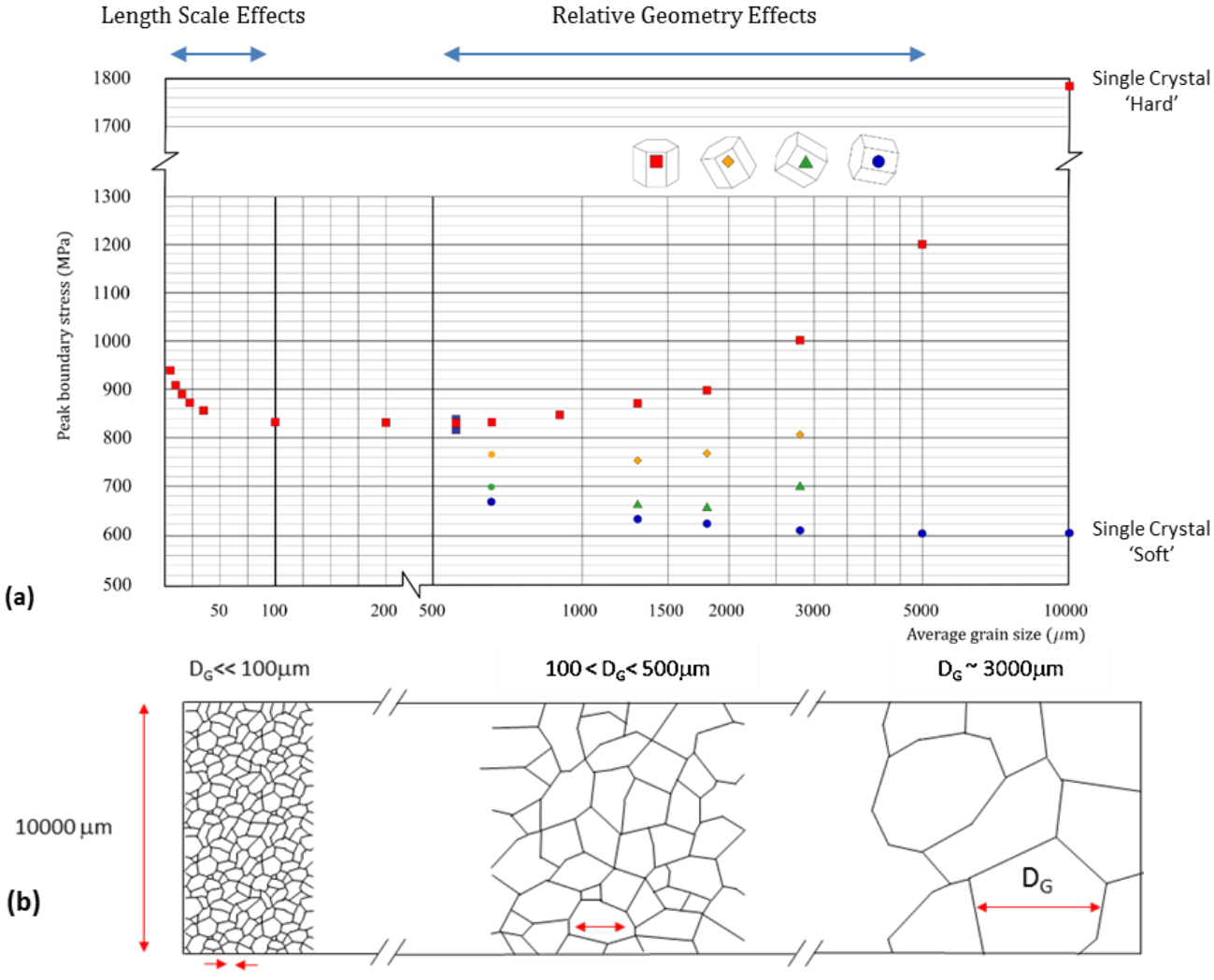

Figure 15 - Overall results showing peak boundary stress across the full range of length scales. The larger grain sizes are plotted on a $\log_{10}$ scale for clarity.

The length scale effects shown in Fig. 15(a) for small AGS show the considerable strengthening due to GNDs. GND densities generate high stresses as a result of the hardening, and it is a strengthening effect

as it inhibits strain accumulation. This is relevant for the understanding of failure in cold dwell fatigue, for example, for which failure is currently thought to result from both localisation of slip at hard-soft gran boundaries, and potentially from stress-based fracture criteria. The small AGS study supports a conclusion that smaller grain sizes are beneficial for dwell fatigue as higher operational stresses would be required to nucleate a facet.

This may be contrasted with the hardening behaviour observed for large AGS on the right hand side of Fig.15 (a) and in Fig. 13. Hardening in this instance is as a result of a build-up of strain in the soft grain. The soft grains surrounding the hard grain yield and once they do, they creep, accumulating large amounts of plastic strain and due to compatibility constraints, there is a consequent local rise in stress in the soft / hard interface. Examining the stress distribution in Fig. 13(a), it may be seen that the large grain sample has much higher boundary stresses and much lower soft grain stresses, than for comparison, the 5μm AGS sample (Fig. 14(a)), where there is a corresponding stress rise in both the soft and hard grain, but less pronounced.

The so-termed relative size effects potentially poses a serious concern for blocky alpha in areas of small ligament width, such as the fillet of a weld in a zirconium fuel clad or the bore of a compressor disk in an aero-engine. Strain accumulation can lead to increased residual stresses at bad pairings of grain orientation due to the elastic and plastic anisotropies of the hcp alpha phase of both titanium and zirconium. The presence of residual stresses that may be higher than design tolerances ultimately affect fatigue life. Accurate prediction of likely residual stress states at the intergranular level is thus of much interest to aeroengine manufacturers and nuclear reactor designers (from discussions with our collaborators in Rolls-Royce plc).

5 Conclusions

This manuscript presents a rigorous physical explanation of the size effect from single crystal studies and then demonstrates how this is important in polycrystals.

Firstly, this paper introduces a fundamental derivation of the back stress term required to harden slip systems according to the mechanism of dislocation pile up. Next, single crystal micro-beam deformation has been considered in order to explore the Gong et al approach for property extraction and length scale dependent crystal plasticity size effects. Finally, model polycrystals are addressed across a broad range of average grain sizes such that both length scale and relative geometry effects (where grain size is a fraction of $1/20^{th}$ or greater of the stress-bearing ligament width) have been examined systematically.

The length scale dependent single crystal micro-beam studies show that:

- The CP model demonstrates that the size effect is most pronounced for effective lengths smaller than 10μm, in agreement with Fleck et al. [4]
- The CP model reproduces qualitatively the observed *A/d* relationship from micro-scale testing (by e.g. Gong et al., Motz et al.)
- The size-sensitive strengthening parameter *A* determined is smaller than experimentally measured, and it is argued that this results from the averaging of discrete dislocation behaviour in to the continuum slip rule required within the crystal plasticity formulation. In addition, decreased volumes have reduced possibilities of dislocation sources, driving up stress. Tarleton et al. [22] suggest that the size effect in micro-beam samples is a combination of GND storage and source limitation or truncation. The latter mechanism is also not accounted for in this crystal model.

Model Ti-6Al polycrystals have also been developed to address size effects originating from both length scale and relative geometry effects. A systematic study of grain size effects in polycrystal behaviour has been carried out in which average grain size is progressively increased from micron scale to millimetres, for a given stress-bearing ligament width. These studies show that:

- For the former micron scale, GND development leads to classical length scale effects while for the latter millimetre scale, for which the grain size becomes a fraction of $1/20^{th}$ or more of the ligament width, relative geometry effects become significant leading to marked impact on material properties and behaviour.
- Considering as an example uniaxial polycrystal straining in a sample of defined ligament width and average grain size, the regimes of grain size for which length scale and relative geometry effects predominate have been demarcated and quantified, thus providing guidelines for alloy users.

Key technological drivers for which such information is important include cold dwell facet fatigue in aero titanium alloys, and blocky alpha zirconium alloys used in nuclear reactor components.

Acknowledgments

We gratefully acknowledge financial support from Rolls-Royce plc and from the Engineering and Physical Sciences Research Council funded *HexMat* programme, grant number EP/K034332/1. TBB acknowledges funding for his fellowship from the Royal Academy of Engineering.

Appendix

A.1 Derivation of back stress and pile-up length relationship

The shear stress field due to an edge dislocation [56] is given as:

$$\sigma_{xy} = \frac{Gb}{2\pi(1-\nu)} \frac{x(x^2-y^2)}{(x^2+y^2)^2} \quad \text{A1}$$

Consider a dipole that consists of two opposite edge dislocations which reach the equilibrium state under the applied shear stress, τ.

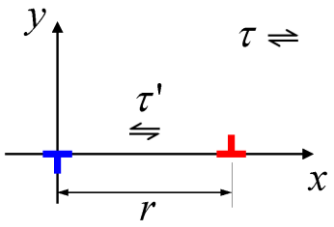

Figure A.1 – Two dislocations of opposite sign

Using Eqn. A1, the shear stress on one dislocation from the other is:

$$\tau' = \frac{Gb}{2\pi(1-\nu)r} \quad \text{A2}$$

in which r is the length of the dipole, noting that x = r and y = 0. At the equilibrium position, the attraction stress is balanced with the applied stress which gives:

$$\tau = \frac{Gb}{2\pi(1-\nu)r} \quad \text{A3}$$

Take the half length of the dipole, i.e. $r/2$, as the unit length and assume N positive edge dislocations are piling up on a slip plane with the angle θ with respect to the positive x-axis. The leading dislocation is pinned at the origin while the rest are free to move along the slip plane under the remote uniaxial loading $\sigma_{xx} = \sigma_0$. The length of the pile up can be solved from the zeros of the derivative of the nth Laguerre polynomial which is given by Stroh [45] as:

$$L_{pu} = 4N \quad \text{A4}$$

Combining A3 and A4, the pile-up length may now be stated as:

$$L_{pu} = \frac{GbN}{\pi(1-\nu)\tau_s} \quad \text{A5}$$

For completeness, the Stroh-based description for the length of a pile-up has been validated with a 2D discrete dislocation (DD) plasticity model.

A two-dimensional discrete dislocation model has been built to validate the analytical solution for the pile-up length L_0 as shown in Fig. A.2. A pile-up group consists of N positive edge dislocations which are distributed evenly along one prism slip plane oriented at $\theta = 60°$. The leading dislocation is fixed at the central node of the model and the rest are free to move along the slip plane. Uniaxial stress-controlled loading is applied along the x-direction. The boundary condition problem is solved using the superposition method developed by Van Der Giessen et al. [57].

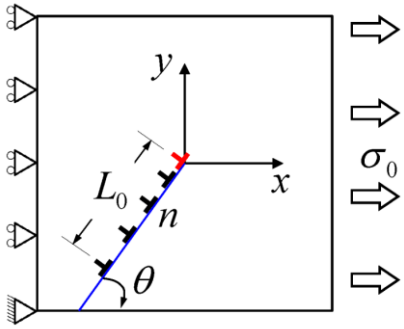

Figure A.2 - Schematic of DD model

In the numerical DD model developed, the region around the pile-up group was highly refined and contains 10^4 elements in a region of 0.5μm × 0.5μm. The region modelled may be considered as an analogous subset of the plastic zone of the beam in bending. An adaptive time step was used to obtain the equilibrium position. The final pile-up distance is recorded versus number of dislocations in the pile-up as shown in Fig. A.3.

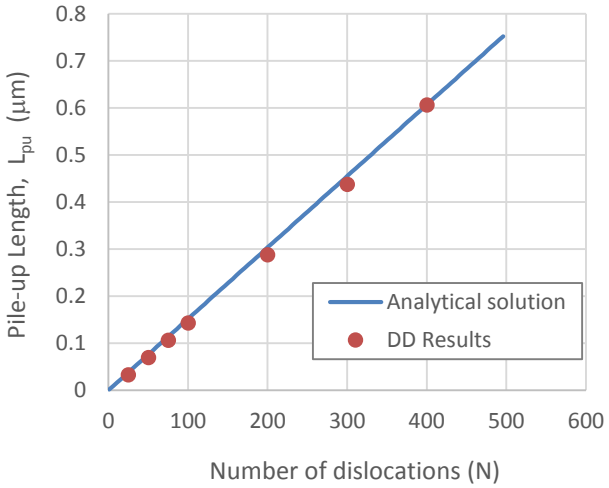

Figure A.3 – Comparison between analytical solution and DD simulations

L_{pu} is shown to be linearly related to the number of dislocation *N* and there is a good agreement between the analytical solution and the DD simulations.

A.2 Elastic moduli

$$\boldsymbol{D} = \begin{bmatrix} 134 & 76 & 65 & 0 & 0 & 0 \\ 76 & 134 & 65 & 0 & 0 & 0 \\ 65 & 65 & 160 & 0 & 0 & 0 \\ 0 & 0 & 0 & 29 & 0 & 0 \\ 0 & 0 & 0 & 0 & 40 & 0 \\ 0 & 0 & 0 & 0 & 0 & 40 \end{bmatrix} GPa$$

Elastic moduli matrix reproduced from Ohio State University experiments on single crystal Ti-6Al **[50]**. The stiffness matrix reproduced here is of the form appropriate for implementation in Abaqus software, noting that (D_{11}- D_{22}) / 2 = D_{44} as appropriate for a transversely isotropic material.

A.3 Slip Rule parameters

Parameters	Value
$\boldsymbol{\rho_{mobile}}^{\mathbf{SSD}}$	5.0 μm^{-2}
$\boldsymbol{\rho_{initial}}^{\mathbf{SSD}}$	0.01 μm^{-2}
$\boldsymbol{\rho_{initial}}^{\mathbf{GND}}$	0.0 μm^{-2}
$\boldsymbol{v}$	1.0 x 10^{11} Hz
b <a>	3.2 x 10^{-4} μm
b <c+a>	5.1 x 10^{-4} μm
ΔH	9.913 x 10^{-20} J
k	1.381x10^{23} J K^{-1}
T	293 K
$\boldsymbol{\gamma_0}$	6x10^{-4}
$\boldsymbol{\gamma'}$	0.05
$\boldsymbol{\tau_0}$ **<a>**	280 MPa
$\boldsymbol{\tau_0}$ **<c+a>**	840 MPa
G	29000 MPa

References

[1] E. Hall, 'The deformation and ageing of mild steel: III. Discussion of results', *Phys Soc Lond*, vol. 64, pp. 747–753, 1951.

[2] N. J. Petch, 'The cleavage strength of polycrystals', *J Iron Steel Inst*, vol. 174, pp. 25–28, 1953.

[3] D. Dunstan and A. Bushby, 'Grain size dependence of the strength of metals: The Hall–Petch effect does not scale as the inverse square root of grain size', *Int. J. Plast.*, vol. 53, pp. 56–65, 2014.

[4] N. A. Fleck, G. M. Muller, M. F. Ashby, and J. W. Hutchinson, 'Strain gradient plasticity: Theory and experiment', *Acta Metall. Mater.*, vol. 42, no. 2, pp. 475–487, Feb. 1994.

[5] J. F. Nye, 'Some geometrical relations in dislocated crystals', *Acta Metall.*, vol. 1, no. 2, pp. 153–162, Mar. 1953.

[6] M. F. Ashby, 'The deformation of plastically non-homogeneous materials', *Philos. Mag.*, vol. 21, no. 170, pp. 399–424, 1970.

[7] N. A. Fleck and J. W. Hutchinson, 'Strain Gradient Plasticity', in *Advances in Applied Mechanics*, vol. 33, J. W. H. and T. Y. Wu, Ed. Elsevier, 1997, pp. 295–361.

[8] A. Arsenlis and D. M. Parks, 'Crystallographic aspects of geometrically-necessary and statistically-stored dislocation density', *Acta Mater.*, vol. 47, no. 5, pp. 1597–1611, Mar. 1999.

[9] S. Sandfeld, M. Monavari, and M. Zaiser, 'From systems of discrete dislocations to a continuous field description: stresses and averaging aspects', *Model. Simul. Mater. Sci. Eng.*, vol. 21, no. 8, p. 085006, Dec. 2013.

[10] M. S. Öztop, C. F. Niordson, and J. W. Kysar, 'Length-scale effect due to periodic variation of geometrically necessary dislocation densities', *Int. J. Plast.*, vol. 41, pp. 189–201, Feb. 2013.

[11] C. F. O. Dahlberg and J. Faleskog, 'Strain gradient plasticity analysis of the influence of grain size and distribution on the yield strength in polycrystals', *Eur. J. Mech. - ASolids*, vol. 44, pp. 1–16, Mar. 2014.

[12] C. F. Niordson and J. W. Kysar, 'Computational strain gradient crystal plasticity', *J. Mech. Phys. Solids*, vol. 62, pp. 31–47, Jan. 2014.

[13] J. R. Mayeur and D. L. McDowell, 'An evaluation of higher-order single crystal strength models for constrained thin films subjected to simple shear', *J. Mech. Phys. Solids*, vol. 61, no. 9, pp. 1935–1954, Sep. 2013.

[14] N. M. Cordero, S. Forest, and E. P. Busso, 'Generalised continuum modelling of grain size effects in polycrystals', *Comptes Rendus Mécanique*, vol. 340, no. 4–5, pp. 261–274, Apr. 2012.

[15] L. H. Poh, R. H. J. Peerlings, M. G. D. Geers, and S. Swaddiwudhipong, 'Towards a homogenized plasticity theory which predicts structural and microstructural size effects', *J. Mech. Phys. Solids*, vol. 61, no. 11, pp. 2240–2259, Nov. 2013.

[16] C. F. O. Dahlberg, Y. Saito, M. S. Öztop, and J. W. Kysar, 'Geometrically necessary dislocation density measurements associated with different angles of indentations', *Int. J. Plast.*, vol. 54, pp. 81–95, Mar. 2014.

[17] A. Ramazani, K. Mukherjee, A. Schwedt, P. Goravanchi, U. Prahl, and W. Bleck, 'Quantification of the effect of transformation-induced geometrically necessary dislocations on the flow-curve modelling of dual-phase steels', *Int. J. Plast.*, vol. 43, pp. 128–152, Apr. 2013.

[18] J. Gong and A. J. Wilkinson, 'Micro-cantilever testing of< a> prismatic slip in commercially pure Ti', *Philos. Mag.*, vol. 91, no. 7–9, pp. 1137–1149, 2011.

[19] J. Gong and A. J. Wilkinson, 'A microcantilever investigation of size effect, solid-solution strengthening and second-phase strengthening for< a> prism slip in alpha-Ti', *Acta Mater.*, vol. 59, no. 15, pp. 5970–5981, 2011.

[20] C. Motz, T. Schöberl, and R. Pippan, 'Mechanical properties of micro-sized copper bending beams machined by the focused ion beam technique', *Acta Mater.*, vol. 53, no. 15, pp. 4269–4279, Sep. 2005.

[21] C. Motz, D. Weygand, J. Senger, and P. Gumbsch, 'Micro-bending tests: A comparison between three-dimensional discrete dislocation dynamics simulations and experiments', *Acta Mater.*, vol. 56, no. 9, pp. 1942–1955, May 2008.

[22] E. Tarleton, D. S. Balint, J. Gong, and A. J. Wilkinson, 'A discrete dislocation plasticity study of the micro-cantilever size effect', *Acta Mater.*, vol. 88, pp. 271–282, Apr. 2015.
[23] R. Ding, J. Gong, A. J. Wilkinson, and I. P. Jones, 'Transmission electron microscopy of deformed Ti–6Al–4 V micro-cantilevers', *Philos. Mag.*, vol. 92, no. 25–27, pp. 3290–3314, Sep. 2012.
[24] R. Ding, J. Gong, A. J. Wilkinson, and I. P. Jones, '< c+a> Dislocations in deformed Ti–6Al–4V micro-cantilevers', *Acta Mater.*, vol. 76, pp. 127–134, 2014.
[25] M. D. Uchic, D. M. Dimiduk, J. N. Florando, and W. D. Nix, 'Sample Dimensions Influence Strength and Crystal Plasticity', *Science*, vol. 305, no. 5686, pp. 986–989, Aug. 2004.
[26] D. M. Dimiduk, M. D. Uchic, and T. A. Parthasarathy, 'Size-affected single-slip behavior of pure nickel microcrystals', *Acta Mater.*, vol. 53, no. 15, pp. 4065–4077, Sep. 2005.
[27] J. R. Greer, W. C. Oliver, and W. D. Nix, 'Size dependence of mechanical properties of gold at the micron scale in the absence of strain gradients', *Acta Mater.*, vol. 53, no. 6, pp. 1821–1830, Apr. 2005.
[28] J. R. Greer and W. D. Nix, 'Nanoscale gold pillars strengthened through dislocation starvation', *Phys. Rev. B*, vol. 73, no. 24, p. 245410, Jun. 2006.
[29] T. B. Britton, F. P. E. Dunne, and A. J. Wilkinson, 'On the mechanistic basis of deformation at the microscale in hexagonal close-packed metals', *Proc. R. Soc. Lond. Math. Phys. Eng. Sci.*, vol. 471, no. 2178, p. 20140881, Jun. 2015.
[30] M. J. Donachie, *Titanium: A Technical Guide, 2nd Edition*. ASM International, 2000.
[31] S. Ghosh, M. Mills, S. Rokhlin, V. Sinha, W. O. Soboyejo, and J. C. Williams, 'The evaluation of cold dwell fatigue in Ti-6242', U.S. Dept. of Transportation / Federal Aviation Authority report, DOT/FAA/AR-06/24, 2007.
[32] S. Williams, 'Private communication, Rolls-Royce plc', Jun-2014.
[33] J. A. Grogan, S. B. Leen, and P. E. McHugh, 'Influence of statistical size effects on the plastic deformation of coronary stents', *J. Mech. Behav. Biomed. Mater.*, vol. 20, pp. 61–76, Apr. 2013.
[34] B. P. Murphy, H. Cuddy, F. J. Harewood, T. Connolley, and P. E. McHugh, 'The influence of grain size on the ductility of micro-scale stainless steel stent struts', *J. Mater. Sci. Mater. Med.*, vol. 17, no. 1, pp. 1–6, Jan. 2006.
[35] C. A. Sweeney, B. O'Brien, F. P. E. Dunne, P. E. McHugh, and S. B. Leen, 'Strain-gradient modelling of grain size effects on fatigue of CoCr alloy', *Acta Mater.*, vol. 78, pp. 341–353, Oct. 2014.
[36] C. A. Sweeney, B. O′Brien, F. P. E. Dunne, P. E. McHugh, and S. B. Leen, 'Micro-scale testing and micromechanical modelling for high cycle fatigue of CoCr stent material', *J. Mech. Behav. Biomed. Mater.*, vol. 46, pp. 244–260, Jun. 2015.
[37] A. Manonukul, F. P. E. Dunne, and D. Knowles, 'Physically-based model for creep in nickel-base superalloy C263 both above and below the gamma solvus', *Acta Mater.*, vol. 50, no. 11, pp. 2917–2931, Jun. 2002.
[38] F. P. E. Dunne, A. Walker, and D. Rugg, 'A systematic study of hcp crystal orientation and morphology effects in polycrystal deformation and fatigue', *Proc. R. Soc. Math. Phys. Eng. Sci.*, vol. 463, no. 2082, pp. 1467–1489, Aug. 2007.
[39] F. P. E. Dunne, D. Rugg, and A. Walker, 'Lengthscale-dependent, elastically anisotropic, physically-based hcp crystal plasticity: Application to cold-dwell fatigue in Ti alloys', *Int. J. Plast.*, vol. 23, no. 6, pp. 1061–1083, Jun. 2007.
[40] F. P. E. Dunne, R. Kiwanuka, and A. J. Wilkinson, 'Crystal plasticity analysis of micro-deformation, lattice rotation and geometrically necessary dislocation density', *Proc. R. Soc. Math. Phys. Eng. Sci.*, vol. 468, no. 2145, pp. 2509–2531, Aug. 2012.
[41] M. E. Kartal, M. A. Cuddihy, and F. P. E. Dunne, 'Effects of crystallographic orientation and grain morphology on crack tip stress state and plasticity', *Int. J. Fatigue*, vol. 61, pp. 46–58, Apr. 2014.
[42] V. V. C. Wan, D. W. MacLachlan, and F. P. E. Dunne, 'A stored energy criterion for fatigue crack nucleation in polycrystals', *Int. J. Fatigue*, vol. 68, pp. 90–102, Nov. 2014.
[43] H. Conrad, 'Thermally activated deformation of α titanium below 0.4 TM', *Can. J. Phys.*, vol. 45, no. 2, pp. 581–590, Feb. 1967.

[44] E. Anderson, Z. Bai, C. Bischof, S. Blackford, J. Demmel, J. Dongarra, J. Du Croz, A. Greenbaum, S. Hammarling, A. McKenney, and D. Sorensen, *LAPACK Users' Guide*, Third. Philadelphia, PA: Society for Industrial and Applied Mathematics, 1999.
[45] A. N. Stroh, 'The Formation of Cracks as a Result of Plastic Flow', *Proc. R. Soc. Lond. Ser. Math. Phys. Sci.*, vol. 223, no. 1154, pp. 404–414, Jun. 1954.
[46] P. D. Littlewood and A. J. Wilkinson, 'Local deformation patterns in Ti–6Al–4V under tensile, fatigue and dwell fatigue loading', *Int. J. Fatigue*, vol. 43, pp. 111–119, Oct. 2012.
[47] J. Jiang, T. B. Britton, and A. J. Wilkinson, 'The orientation and strain dependence of dislocation structure evolution in monotonically deformed polycrystalline copper', *Int. J. Plast.*, vol. 69, pp. 102–117, Jun. 2015.
[48] G. Lütjering and J. J. C. Williams, *Titanium :* Springer, 2007.
[49] S. Balasubramanian, 'Polycrystalline plasticity : application to deformation processing of lightweight metals', Ph.D. Thesis, Massachusetts Institute of Technology, 1998.
[50] V. Hasija, S. Ghosh, M. J. Mills, and D. S. Joseph, 'Deformation and creep modeling in polycrystalline Ti–6Al alloys', *Acta Mater.*, vol. 51, no. 15, pp. 4533–4549, Sep. 2003.
[51] Z. Zhang, M. A. Cuddihy, and F. P. E. Dunne, 'On rate-dependent polycrystal deformation: the temperature sensitivity of cold dwell fatigue', *Proc R Soc A*, vol. 471, no. 2181, Sep. 2015.
[52] J. Gong and A. J. Wilkinson, 'Anisotropy in the plastic flow properties of single-crystal α titanium determined from micro-cantilever beams', *Acta Mater.*, vol. 57, no. 19, pp. 5693–5705, Nov. 2009.
[53] J. Gong, T. Benjamin Britton, M. A. Cuddihy, F. P. E. Dunne, and A. J. Wilkinson, '⟨a⟩ Prismatic, ⟨a⟩ basal, and ⟨c+a⟩ slip strengths of commercially pure Zr by micro-cantilever tests', *Acta Mater.*, vol. 96, pp. 249–257, Sep. 2015.
[54] D. Rugg, T. B. Britton, J. Gong, A. J. Wilkinson, and P. A. J. Bagot, 'In-service materials support for safety critical applications – A case study of a high strength Ti-alloy using advanced experimental and modelling techniques', *Mater. Sci. Eng. A*, vol. 599, pp. 166–173, Apr. 2014.
[55] M. Sauzay, J. Liu, F. Rachdi, L. Signor, T. Ghidossi, and P. Villechaise, 'Physically-based simulations of the cyclic behavior of FCC polycrystals', *Adv Mat Res*, pp. 891–892, 2014.
[56] J. P. Hirth and J. Lothe, *Theory of Dislocations*. Krieger Publishing Company, 1982.
[57] E. V. der Giessen and A. Needleman, 'Discrete dislocation plasticity: a simple planar model', *Model. Simul. Mater. Sci. Eng.*, vol. 3, no. 5, p. 689, Sep. 1995.